NRC Research Press

ARTICLE

Mapping black ash dominated stands using geospatial and forest inventory data in northern Minnesota, USA

Peder S. Engelstad, Michael J. Falkowski, Anthony W. D'Amato, Robert A. Slesak, Brian J. Palik, Grant M. Domke, and Matthew B. Russell

Can. J. For. Res. Downloaded from www.nrcresearchpress.com by UNIVERSITY OF VERMONT on 08/23/19
For personal use only.

Abstract: Emerald ash borer (EAB; *Agrilus planipennis* Fairmaire, 1888) has been a persistent disturbance for ash forests in the United States since 2002. Of particular concern is the impact that EAB will have on the ecosystem functioning of wetlands dominated by black ash (*Fraxinus nigra* Marsh.). In preparation, forest managers need reliable and complete maps of black ash dominated stands. Traditionally, forest survey data from the United States Forest Inventory and Analysis (FIA) Program have provided rigorous measures of tree species at large spatial extents but are limited when providing estimates for smaller management units (e.g., stands). Fortunately, geospatial data can extend forest survey information by generating predictions of forest attributes at scales finer than those of the FIA sampling grid. In this study, geospatial data were integrated with FIA data in a randomForest model to estimate and map black ash dominated stands in northern Minnesota in the United States. The model produced low error rates (overall error = 14.5%; area under the curve (AUC) = 0.92) and was strongly informed by predictors from soil saturation and phenology. These results improve upon FIA-based spatial estimates at national extents by providing forest managers with accurate, fine-scale maps (30 m spatial resolution) of black ash stand dominance that could ultimately support landscape-level EAB risk and vulnerability assessments.

Key words: compound topographic index (CTI), remote sensing, black ash, emerald ash borer, forest inventory.

Résumé : L'agrile du frêne (AF; *Agrilus planipennis* Fairmaire, 1888) est une source de perturbation persistante dans les forêts de frêne depuis 2002 aux États-Unis. L'impact que l'AF aura sur le fonctionnement de l'écosystème des milieux humides dominés par le frêne noir (*Fraxinus nigra* Marsh.) est particulièrement préoccupant. Pour se préparer, les gestionnaires forestiers ont besoin de cartes exhaustives et fiables des peuplements dominés par le frêne noir. Traditionnellement, les données d'inventaire forestier du programme d'analyse et d'inventaire forestier (AIF) des États-Unis ont fourni des mesures rigoureuses concernant les espèces arborescentes pour de vastes étendues mais elles sont limitées lorsqu'il s'agit de fournir des estimations pour de plus petites unités d'aménagement (p. ex des peuplements). Heureusement, les données géospatiales peuvent étendre la portée des informations de l'inventaire forestier en générant des prédictions des attributs forestiers à des échelles plus fines que la grille d'échantillonnage du programme d'AIF. Dans cette étude, des données géospatiales ont été intégrées avec des données du programme d'AIF dans une forêt d'arbres décisionnels pour estimer et cartographier les peuplements dominés par le frêne noir dans le nord du Minnesota, aux États-Unis. Le modèle a produit de faibles taux d'erreur (erreur globale = 14,5 %; surface sous la courbe (AUC) = 0,92) et était fortement informé par des prédicteurs ayant trait à la saturation du sol et à la phénologie. Ces résultats améliorent les estimations spatiales fondées sur le programme d'AIF à l'échelle nationale en fournissant aux gestionnaires forestiers des cartes précises et à petite échelle (résolution spatiale de 30 m) des peuplements dominés par le frêne noir qui pourraient en fin de compte servir de base à l'évaluation des risques et de la vulnérabilité à l'AL. [Traduit par la Rédaction]

Mots-clés : indice topographique composé (CTI), télédétection, frêne noir, agrile du frêne, inventaire forestier.

1. Introduction

A variety of exotic flora, fauna, and pathogens induce ecological changes to forest ecosystems worldwide, ultimately disrupting ecosystem processes and functions, including nutrient cycling, productivity, and wildlife habitat (Lovett et al. 2016). In the short term, some invasive species can alter forest floor environments and create canopy gaps, whereas long-term changes may affect entire forest successional trajectories (Gandhi and Herms 2010). One such invasive species is the emerald ash borer (EAB; *Agrilus planipennis* Fairmaire, 1888), a wood-boring beetle that was first discovered in southeast Michigan in 2002. EAB has been found to attack all ash species with >2.5 cm diameter, regardless of health (Herms and McCullough 2014), and kills hosts in as little as 2 years (Knight et al. 2013). Because of widespread municipal planting of ash trees, much of the research on EAB impact and mitigation strategies has been restricted to urban environments (i.e., Crook et al. 2008; Poland and McCullough 2006; Kovacs et al. 2011). However, EAB range expansion and the associated threat to nonurban

Received 8 November 2018. Accepted 3 March 2019.

P.S. Engelstad and M.J. Falkowski. Natural Resource Ecology Laboratory, Colorado State University, Fort Collins, CO 80523, USA.
A.W. D'Amato. Rubenstein School of Environment and Natural Resources, University of Vermont, Burlington, VT 05405, USA.
R.A. Slesak. Minnesota Forest Resources Council, St. Paul, MN 55108, USA; Department of Forest Resources, University of Minnesota, St. Paul, MN 55108, USA.
B.J. Palik. Northern Research Station, USDA Forest Service, Grand Rapids, MN 55744, USA.
G.M. Domke. Northern Research Station, Forest Inventory and Analysis, USDA Forest Service, St. Paul, MN 55108, USA.
M.B. Russell. Department of Forest Resources, University of Minnesota, St. Paul, MN 55108, USA.
Corresponding author: Peder S. Engelstad (email: pengel@colostate.edu).
Copyright remains with the author(s) or their institution(s). Permission for reuse (free in most cases) can be obtained from RightsLink.

Can. J. For. Res. Downloaded from www.nrcresearchpress.com by UNIVERSITY OF VERMONT on 08/23/19
For personal use only.

ash forests is expected to grow because of migrating populations (Taylor et al. 2010), firewood transportation (BenDor et al. 2006), and warming climate conditions (Liang and Fei 2014).

One ash species of particular concern is black ash (*Fraxinus nigra* Marsh.), a slow-growing hardwood tree often found in relatively pure stands on poorly drained soils and in wetlands of the Upper Midwest region of the United States (USA). The native range of black ash spans from western Newfoundland to southeastern Manitoba (Canada), south to Iowa and Ohio, and east to northern Virginia (Wright and Rauscher 1990). Black ash is considered to function as a foundational tree species and thereby strongly regulates ecosystem processes (Ellison et al. 2005; Youngquist et al. 2017). Rapid stand mortality of black ash from EAB attack is expected to have substantial impacts on ecosystem structure and function (Slesak et al. 2014). Indeed, dramatic disruptions are anticipated in native plant communities and wildlife food webs (DeSantis et al. 2013; Looney et al. 2017; Youngquist et al. 2017), biogeochemical processes (Flower et al. 2013), and resistance to invasion by exotic flora (Kenis et al. 2009; Klooster et al. 2014). Additionally, the reduction in evapotranspiration accompanying the loss of black ash may shift vegetation types in these communities from wetland forests to marshlike ecosystems (Diamond et al. 2018) and may ultimately increase flood risk (Telander et al. 2015). The loss of black ash also poses a distinct threat to the cultural practices of multiple Indigenous groups in the northern Great Lakes states by reducing wood sources traditionally used for basketmaking (Costanza et al. 2017; Willow 2011).

To help proactively address these risks and implement mitigation strategies (i.e., planting replacement tree species, employing adaptive silvicultural techniques, and releasing biological controls), forest managers need reliable and complete maps depicting the spatial configuration, extent, and distribution of black ash dominated forests. Large-area estimates of tree species distributions can be generated from systematic forest inventory data collected across large geographic extents (i.e., Blackard et al. 2008); however, such data do not provide specific predictions of species occurrence at spatial extents smaller than that of the systematic sampling grid (McRoberts and Tomppo 2007). The United States Department of Agriculture's Forest Inventory and Analysis (FIA) Program provides forest inventory information through annual surveys of permanent sample plots (Bechtold and Patterson 2005). The strategic-level sampling methodology of FIA ensures that population estimates at county, state, regional, and national levels meet specific precision standards. However, smaller spatial units (e.g., forest district management units and stands) often contain an insufficient number of plots to generate precise local estimates of forest attributes and descriptions of their spatial characteristics (Goerndt et al. 2013). These local estimates of forest conditions are needed to quantify the effects of forest health agents (e.g., EAB) because stands of varying host-tree (e.g., black ash) composition are expected to be differentially affected.

Fortunately, this problem of small-area estimation has been successfully addressed in previous studies by combining FIA data with predictors obtained from a variety of remote sensing sources to generate spatial predictions of forest attributes in the geographic space between FIA survey locations. For example, multispectral data from passive optical sensors (ranging from 5 to 30 m spatial resolution) have been leveraged to estimate basal area (McRoberts and Tomppo 2007), forest disturbance (Schroeder et al. 2014), stand density (McRoberts 2009), successional stage (Liu et al. 2008), and canopy cover (Coulston et al. 2012), among others. Active remote sensing techniques such as light detection and ranging (LiDAR) have also been used in conjunction with data from FIA to predict biomass (Andersen et al. 2009), stand volume (Sheridan et al. 2014), and fire effects (Alonzo et al. 2017).

Species occurrence data from FIA have also been used to classify forest types and are often combined with multiple remote sensing or geospatial resources that help define the biotic and abiotic niches of target species. For example, Evans and Cushman (2009) used topographic indices and Landsat data to estimate the occupancy of four conifer species in northern Idaho. In Maine, Dunckel et al. (2015) mapped eastern hemlock (*Tsuga canadensis* (L.) Carrière) occurrence by combining climate, soil, and topographic indices with Landsat data. In Utah, Zimmermann et al. (2007) compared the effectiveness of topographic and bioclimatic predictors with vegetation indices from Landsat for species-level classification of over a dozen tree species. Similar approaches may be particularly effective in mapping black ash given its common occurrence in wetlands and unique phenology compared with other tree species.

In this study, spectral and topographic indices and auxiliary geospatial layers were combined with data from FIA field surveys to classify black ash dominated stands across a diverse forest landscape in northern Minnesota, USA. It was hypothesized that predictors related to soil moisture and phenology could serve as novel predictors to capture the unique ecology of black ash and that this could help to develop accurate estimates and maps of the location, extent, and distribution of black ash dominated stands. In the development of this approach, a model selection procedure was used to evaluate the most important predictors for classifying black ash stands and generate a highly accurate, parsimonious model that accounted for class imbalance. Model performance was evaluated via traditional accuracy assessment statistics and by conditional density plots to determine if the model produced ecologically meaningful results. Furthermore, a spatial assessment of classification stability was performed to explore the potential sources of error when classifying stand dominance across a diverse array of forest conditions.

2. Methods

2.1. Study area

The study area is defined by the extent of a Landsat scene (WRS-2 Path 28/Row 27) in northern Minnesota (Fig. 1). The area (~36 000 km^2) sits on the transition zone between boreal and mixed forest types resulting in a diverse, heterogeneous mix of hardwood and conifer species that occur in well-drained uplands and poorly drained swamps and bogs. Historical climate records (1981–2010) indicate a mean annual precipitation of 540 to 810 mm (Minnesota Department of Natural Resources 2017), and elevation ranges from ~350 to 600 m above sea level. The study area contains a mix of public and private lands, including the entirety of Chippewa National Forest. The study area was selected because of the availability of statewide LiDAR products in Minnesota and cloud-free Landsat imagery coterminous with the most recent year of publicly accessible FIA data. Placing the study in the forests of northern Minnesota is also relevant because of its proximity to ongoing EAB outbreaks and associated urgency for adaptive management strategies for black ash forests (D'Amato et al. 2018), as well as the predicted northward shifts in EAB range (Liang and Fei 2014).

2.2. Data collection

Field data used in this study consisted of 1765 FIA plots measured during a single inventory cycle between 2011 and 2015. The sampling design of FIA consists of long-term survey sites systematically stratified across public and private lands, with each site consisting of four 0.02 ha fixed-radius subplots (i.e., phase 2 plots; Bechtold and Patterson 2005). The large number of forest attributes collected at each site generally fall into two categories: site description and direct measurement. Site descriptions include observations of forest type, condition (e.g., forest or nonforest), and disturbance. Measurements recorded at the individual-tree level include standard forestry metrics such as diameter at breast height (DBH; breast height = 1.35 m), tree height, age, and species.

Can. J. For. Res. Downloaded from www.nrcresearchpress.com by UNIVERSITY OF VERMONT on 08/23/19
For personal use only.

Fig. 1. Spatial extent of the study area in northern Minnesota. Forest Inventory and Analysis (FIA) plots (n = 1765) evaluated during model development are shown for the 2011–2015 data collection cycle. As displayed, plot locations are "fuzzed" (within 0.8 km of true locations) for privacy purposes, but true plot coordinates were used during model development via an agreement with FIA. Surface water is shown in darker gray.

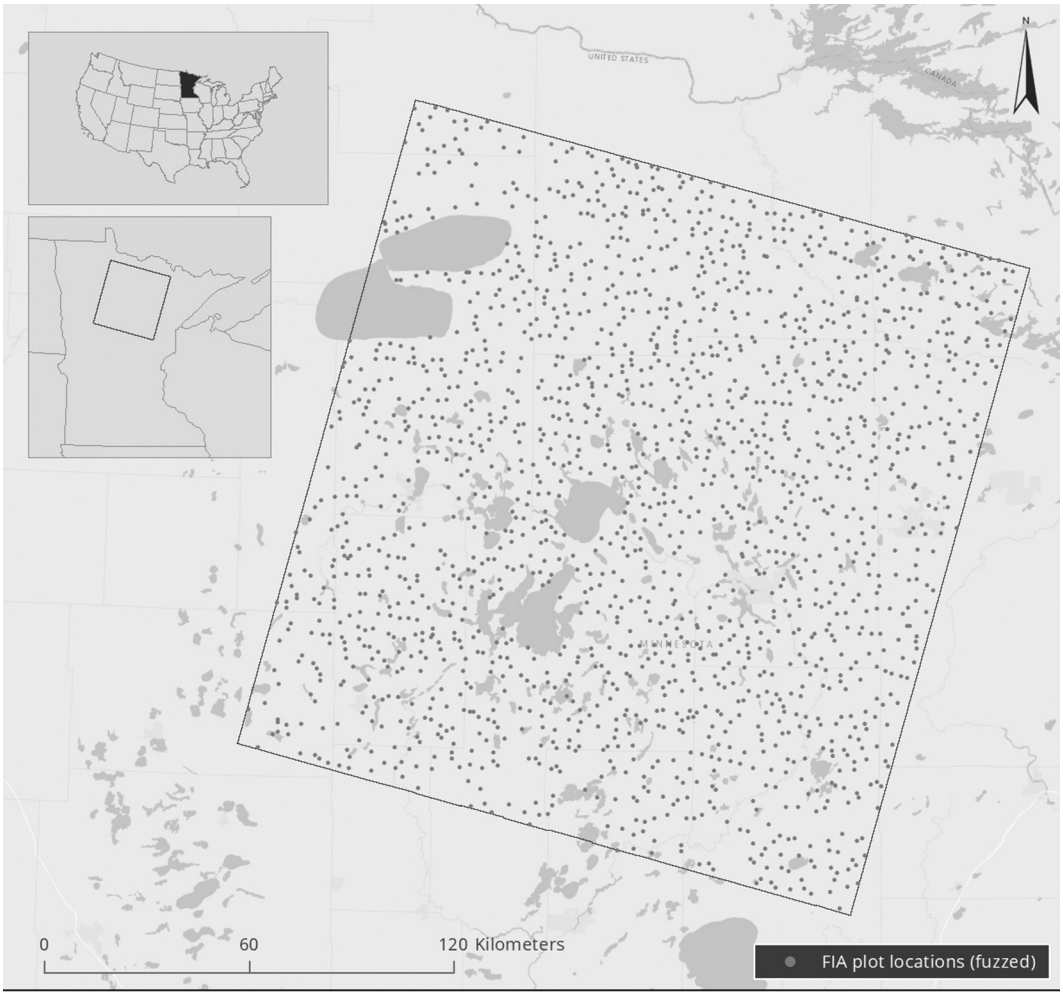

To quantify stand dominance, basal area was calculated for each species using DBH. Basal area is understood as a correlate of stand density and has been successfully used in previous remote sensing studies of forest species occurrence (Duveneck et al. 2015; Goerndt et al. 2013; Martin et al. 1998; Moisen et al. 2006; Ohmann and Gregory 2002). Total basal area for the plot was determined by scaling to the hectare level using an expansion factor listed in the FIA database for living trees ≥ 12.7 cm DBH. The relative dominance for each species in the plot was calculated as the total basal area by species divided by the total plot basal area.

To explore a measure of stand dominance, plots with a simple majority of black ash (≥50% of total plot basal area) were assigned a binary value of presence (1), whereas plots where black ash accounted for less than 50% of total basal area were assigned a value of absence (0). From the 1765 field plots available during the inventory cycle, 923 remained after retaining only undisturbed, forested plots with single land cover condition. The application of the stand-dominance threshold resulted in training data that included 874 absence and 49 presence points.

2.3. Remote sensing data

The use of active and passive remote sensing data is common in ecological research. Specific to species-level classification, these data can potentially describe the biophysical characteristics of the target species' environmental niche and growth patterns. For this study, a LiDAR-derived digital terrain model (MNGeo 2017) was used to derive 20 m spatial resolution topographic indices to describe a variety of soil attributes (Table 1). To characterize the wet soils typical of black ash stands, indices were chosen that reflect soil moisture potential (compound topographic index, CTI), solar temperature effects (heat load index; McCune and Keon 2002), and water-holding capacity (integrated moisture index; Iverson et al. 1997), in addition to standard topography metrics such as elevation, slope, and aspect.

Although LiDAR point-cloud data can be extremely useful for characterizing forest structure, the low-density data set used in this study was not explicitly designed for assessing vegetation structure; rather, acquisition parameters were optimized for topographic mapping. Thus, acquisition parameters such as scan angle, flight-line overlap, and point density are far below recommended thresholds for vegetation mapping and structural assessment (e.g., Evans et al. 2009). Fortunately, multispectral satellite sensors collect data with higher spectral and temporal resolution, facilitating species differentiation and the computation of seasonal means from vegetation indices. In this study, Landsat 8 single-date (13 September 2015), cloud-free, surface-reflectance vegetation indices were acquired from the U.S. Geological Survey (USGS 2017; Table 1) at a 30 m spatial resolution.

Can. J. For. Res. Downloaded from www.nrcresearchpress.com by UNIVERSITY OF VERMONT on 08/23/19
For personal use only.

Table 1. The 44 candidate predictor variables evaluated during development of the randomForest classification of black ash stand dominance in northern Minnesota.

Source	Variable	Description
LiDAR DTM (20 m)	**CTI**	Compound topographic index
LiDAR DTM (20 m)	CURVE	Slope curvature
Landsat (30 m)	**doy_EVI**	Single-date enhanced vegetation index
Landsat (30 m)	doy_IFZ	Single-date integrated forest Z score
Landsat (30 m)	doy_MSAVI	Single-date modified soil-adjusted vegetation index
Landsat (30 m)	**doy_NBR**	Single-date normalized burn ratio
Landsat (30 m)	**doy_NDMI**	Single-date normalized difference moisture index
Landsat (30 m)	doy_NDVI	Single-date normalized difference vegetation index
Landsat (30 m)	doy_SAVI	Single-date soil-adjusted vegetation index
Landsat (30 m)	**dNBR**	Summer minus fall median differenced normalized burn ratio
Landsat (30 m)	dNDMI	Summer minus fall median normalized difference moisture index
Landsat (30 m)	dNDVI	Summer minus fall median normalized difference vegetation index
LiDAR DTM (20 m)	ELEV	Elevation (m)
Landsat (30 m)	fall_NBR	Median normalized burn ratio (September–October)
Landsat (30 m)	fall_NDMI	Median normalized difference moisture index (September–October)
Landsat (30 m)	fall_NDVI	Median normalized difference vegetation index (September–October)
Landsat (30 m)	grow_NBR	Median normalized burn ratio (April–October)
Landsat (30 m)	grow_NDMI	Median normalized difference moisture index (April–October)
Landsat (30 m)	grow_NDVI	Median normalized difference vegetation index (April–October)
LiDAR DTM (20 m)	HLI	Heat load index
LiDAR DTM (20 m)	IMI	Integrated moisture index
Landsat (30 m)	JSmax_NBR	Maximum normalized burn ratio (June–September)
Landsat (30 m)	JSmax_NDMI	Maximum normalized difference moisture index (June–September)
Landsat (30 m)	JSmax_NDVI	Maximum normalized difference vegetation index (June–September)
Landsat (30 m)	JSmin_NBR	Minimum normalized burn ratio (June–September)
Landsat (30 m)	**JSmin_NDMI**	Minimum normalized difference moisture index (June–September)
Landsat (30 m)	JSmin_NDVI	Minimum normalized difference vegetation index (June–September)
Landsat (30 m)	JSmed_NBR	Median normalized burn ratio (June–September)
Landsat (30 m)	JSmed_NDMI	Median normalized difference moisture index (June–September)
Landsat (30 m)	JSmed_NDVI	Median normalized difference vegetation index (June–September)
LiDAR DTM (20 m)	ROUGH	Terrain roughness
SSURGO (30 m)	SOILS_DI	SSURGO soil drainage index
SSURGO (30 m)	SOILS_PI	SSURGO soil productivity index
Landsat (30 m)	summ_NBR	Summer normalized burn ratio (July–August)
Landsat (30 m)	summ_NDMI	Summer normalized difference moisture index (July–August)
Landsat (30 m)	summ_NDVI	Summer normalized difference vegetation index (July–August)
Landsat (30 m)	**TCAP_A**	Harmonized tasseled cap angle
Landsat (30 m)	**TCAP_B**	Harmonized tasseled cap brightness (Vogeler et al. 2018)
Landsat (30 m)	TCAP_D	Harmonized tasseled cap distance
Landsat (30 m)	**TCAP_DI**	Harmonized tasseled cap disturbance index
Landsat (30 m)	**TCAP_G**	Harmonized tasseled cap greenness (Vogeler et al. 2018)
Landsat (30 m)	**TCAP_W**	Harmonized tasseled cap wetness (Vogeler et al. 2018)
LiDAR DTM (20 m)	TRASP	Transformed aspect
NWI (30 m)	**WETLAND**	National Wetlands Inventory category

Note: Variables included in the final model are indicated in boldface type. LiDAR, light detection and ranging; DTM, digital terrain model; SSURGO, Soil Survey Geographic Database; NWI, National Wetlands Inventory.

Additionally, Google Earth Engine (https://earthengine.google.com) was used to generate minimum, maximum, median, and differenced values for normalized burn ratio (NBR), normalized difference vegetation index (NDVI), and normalized difference moisture index (NDMI) at a 30 m spatial resolution (Table 1) within a date range long enough to capture the growth cycles of multiple forest species (1 April to 31 October 2015). The goal of including seasonally descriptive predictors was to differentiate the phenological signature of black ash, defined by smaller annual leaf-area growth and a restricted number of growing days (Telander et al. 2015) from co-occurring deciduous tree species.

2.4. Auxiliary geospatial data

To further capture the abiotic niche of black ash, geospatial data were acquired from the National Wetlands Inventory (NWI), which uses manual interpretation of aerial imagery (1 m spatial resolution) to produce a detailed hierarchical classification of wetland habitat types (Dahl et al. 2009). Following previous research establishing forest wetlands as the primary habitat of black ash (Wright and Rauscher 1990), NWI vector data were used to develop a 30 m spatial resolution categorical raster (Table 1) that would discriminate forested from nonforested wetlands. Soil indices (Table 1) from the Soil Survey Geographic Database (SSURGO; Soil Survey Staff 2017) also provided 30 m spatial resolution rasters of soil inundation and nutrient quality. First, a drainage index, designed to measure long-term soil wetness, was used to relate black ash with heavily inundated soils. Second, the incorporation of a productivity index, interpreted from soil taxonomy, provided a measure related to the nutrient content of soils where black ash is found.

2.5. Predictor variable development

FIA plots are located on their own grid system irrespective of any predictor variable georegistration present in this study. To address this, a 3 × 3 focal mean moving window was applied to generate mean values for all continuous predictor variables over the area encompassing all four FIA subplots (~90 m × 90 m) while resampling the predictor rasters to a common spatial resolution

Can. J. For. Res. Downloaded from www.nrcresearchpress.com by UNIVERSITY OF VERMONT on 08/23/19
For personal use only.

(30 m × 30 m). Despite the potential to describe only general forest conditions, this method has been used to partially alleviate coregistration errors between remotely sensed predictors and FIA data incorporating all four subplots (Dunckel et al. 2015; Moisen et al. 2006; Nelson et al. 2009; Powell et al. 2010). An additional consequence of using all four subplots is a potential reduction in training data size if filtering out nonhomogeneous forest-cover classes (McRoberts 2009).

2.6. Model development

A presence and absence classification model of black ash stand dominance was developed using the randomForest algorithm (RF; Breiman 2001) as implemented in the randomForest package (Liaw and Wiener 2002) of the R statistical software (R Core Team 2017). The RF model was run with 4000 bootstrapped replicates (ntrees), with replacement, to reach convergence on error rates and stabilize variable importance and variable interaction (Evans and Cushman 2009). Although RF is considered robust to collinearity (Cutler et al. 2007), a model-selection procedure was used to reduce the number of redundant predictors while retaining ecological interpretability (Falkowski et al. 2009). Prior to model selection, a Gram-Schmidt QR decomposition procedure, which is in the R rfUtilities package (Evans et al. 2011), was used to identify and remove multicollinear predictor variables. To further optimize model parsimony, a model-selection function, also available in rfUtilities, was implemented based on its successful use in previous studies (i.e., Falkowski et al. 2009; Olaya-Marin et al. 2013; Tinkham et al. 2014). This function iterates through and evaluates potential models (i.e., suites of potential predictor variables) by assessing possible variable combinations and comparing them based on a model improvement ratio statistic (Murphy et al. 2010) that measures the difference in percent change in overall out-of-bag error.

2.7. Addressing class imbalance

In machine learning, class-size imbalance remains a regular source of bias, often resulting in the majority class being favored over the minority class (He and Garcia 2009; Japkowicz and Stephen 2002). Specific to RF, the iterative bootstrap sample of training data often lacks a representative sample from the minority class. To address this, downsampling the majority class has previously been shown to be more effective in overcoming majority-class bias when compared with oversampling and weighted class methods (Chen et al. 2004; Drummond and Holte 2003). In this study, the majority class (i.e., absence) was downsampled to match the size of the minority class (i.e., presence; n = 49) for each bootstrap sample to minimize bias from class imbalance.

2.8. Accuracy assessment and model evaluation

Classification accuracy was measured based on internal error estimates from out-of-bag samples generated by the RF model. Overall accuracy and errors of omission and commission were calculated to explore the accuracy of presence and absence classes produced by the model. The model was also assessed using the area under the curve (AUC) statistic, generated from a receiver operating characteristic (ROC) curve comparing the true positive rate (sensitivity) with the true negative rate (specificity). Following this, the model was applied to the geospatial data sets to produce a binary classification of presence and absence of black ash dominance across the study area. Additionally, a class probability map (following Falkowski et al. 2009) was created by assigning the maximum value from the binary model's RF class vote matrix for each cell across the study area. For example, if a grid cell received 80% of the RF votes for a particular class, it would be assigned a value of 0.80. The class probability map was used in conjunction with high spatial resolution imagery (1 m) to visually assess the quality of model predictions. Finally, conditional density plots, which display the probability of class occurrence across the range of values for a single predictor, were examined for the most important predictors (identified by the final RF model) to verify the production of an ecologically reasonable model.

Table 2. Classification accuracy statistics for the randomForest model of presence and absence of black ash stand dominance.

Class	Omission error (producer)	Commission error (user)	Class accuracy (%)
Presence	4.7	14.3	85.7
Absence	24.7	14.6	85.4
Overall accuracy (%)	85.5		

Fig. 2. Plot of variable importance values for the predictors used in the final randomForest model of black ash dominated stand presence or absence. Percent Mean Decrease Accuracy measures the percent accuracy lost with the removal of individual predictor variables (listed on the y axis). See Table 1 for definitions of the abbreviations.

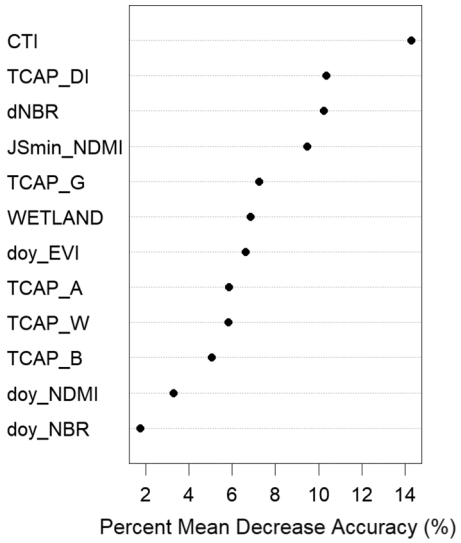

3. Results

3.1. Model selection

The Gram-Schmidt QR decomposition procedure identified and removed 33 multicollinear predictors. The secondary model selection function (model improvement ratio statistic) did not identify further model parsimony optimizations for the binary classification of black ash dominated stands. This left 12 predictor variables that were used to develop the RF classification model: CTI, summer minus fall median differenced NBR (dNBR), June–September minimum NDMI (JSmin_NDMI), tasseled cap (TC) angle, TC brightness, TC greenness, TC wetness, TC disturbance index (TCAP_DI), single-date NBR, single-date enhanced vegetation index (EVI), single-date NDMI, and NWI wetland class (Table 1).

3.2. Classification accuracy and variable importance

The overall accuracy of the final model was 85.5%, and the AUC value was 0.92. Individual class and omission and commission errors were low (Table 2); however, some confusion did occur in the form of false positives, resulting in a 24.7% error rate. The investigation of variable importance (Fig. 2) indicated CTI as the most important, followed closely by TCAP_DI, dNBR, and JSmin_NDMI.

Fig. 3. Binary classification (left), maximum class probability (classification stability) map (right; both 30 m resolution), and associated output summary statistics produced by the randomForest model of black ash stand dominance in northern Minnesota. The color of each bar corresponds to the associated stability level in the legend and probability map. The numbers listed above each bar represent the percentages of total land area for each probability level in the study area.

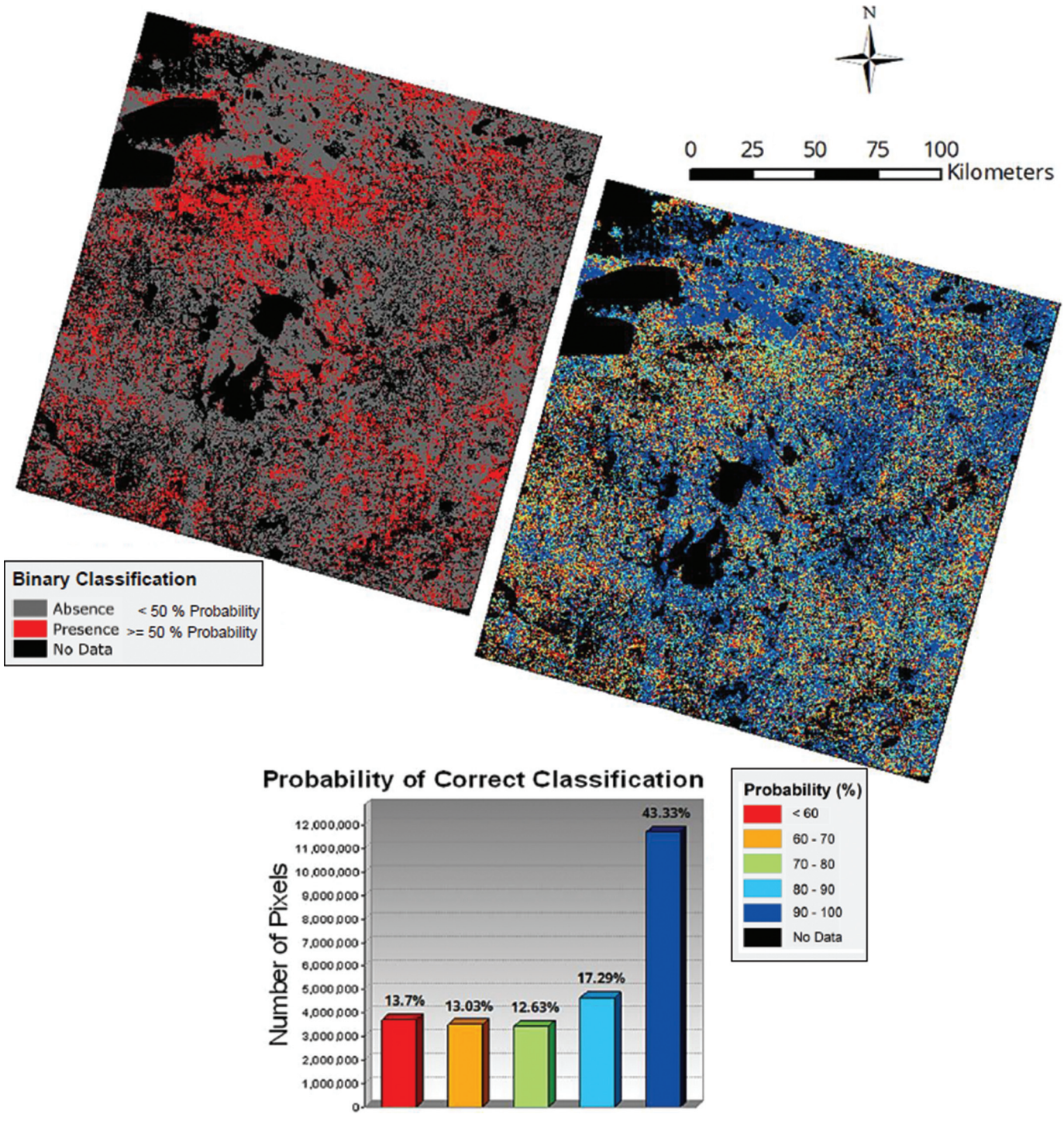

3.3. Model evaluation

The class probability map (Fig. 3) illustrates the prediction stability of both presences and absences. The majority of the study area (~60%) had a classification stability of over 80%. In contrast, approximately 14% of the study area was represented by stability under 60%. Initial visual interpretation of these pixels indicated that higher instability typically occurred in areas of forest disturbance (i.e., harvest) during the years of data collection (Fig. 4). Conditional density plots (Fig. 5) were examined to verify that the model produced ecologically meaningful results. The plots represent the relationships among the probability of presence or absence classes and the four most important predictors. For the presence class, an increasing likelihood of presence is generally associated with increasing values of CTI, TCAP_DI, and dNBR. The inverse is true for JSmin_NDMI, with the likelihood of presence quickly decreasing for values above ~0.25.

Can. J. For. Res. Downloaded from www.nrcresearchpress.com by UNIVERSITY OF VERMONT on 08/23/19
For personal use only.

Fig. 4. Detailed views of the full class probability map (left) overlaying the extent of a known area of forest disturbance (harvest activity) occurring during the FIA data collection cycle (2011–2015). High-resolution (1 m) DigitalGlobe imagery (right) was visually assessed in Google Earth Pro to investigate areas of low prediction stability.

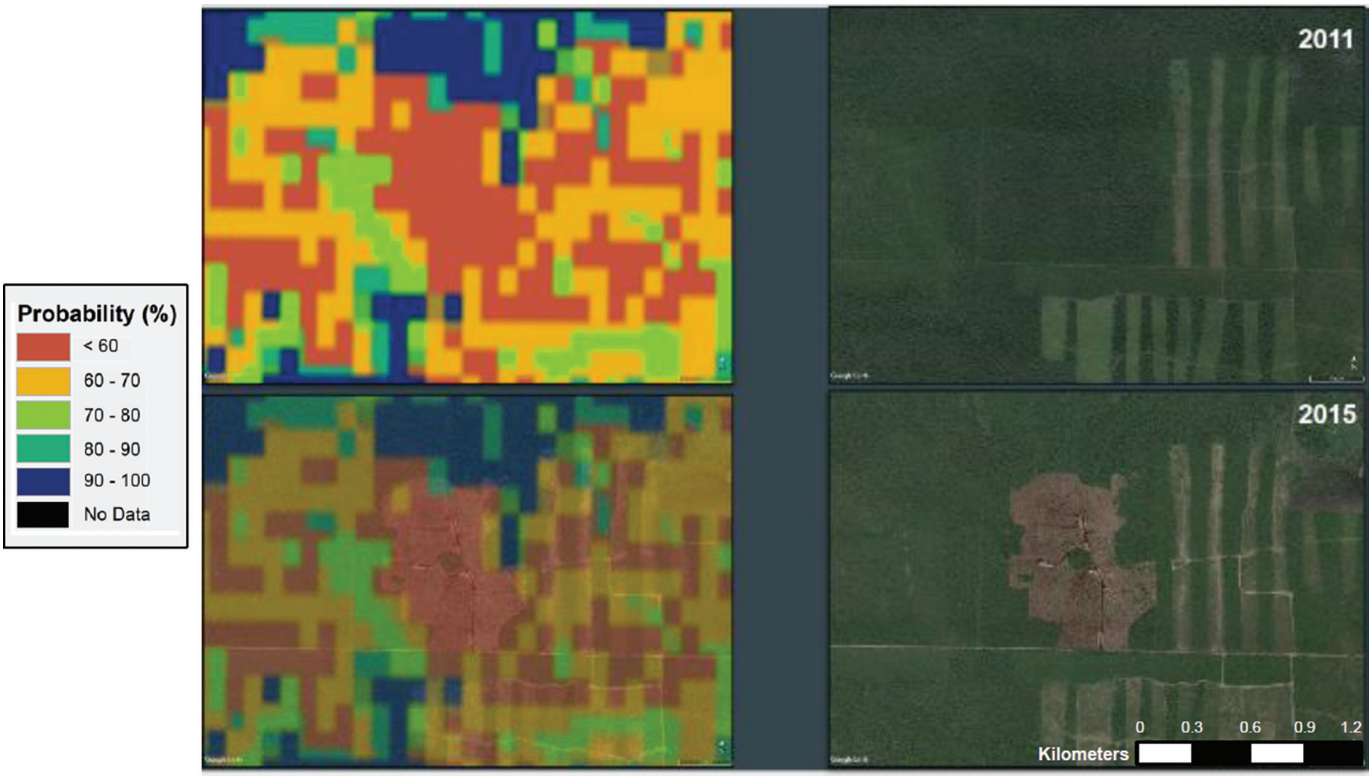

Fig. 5. Conditional density plots for the top four predictors from the randomForest model. The light gray area represents the probability of presence and the dark gray area represents the probability of absence across the range of values for each individual predictor.

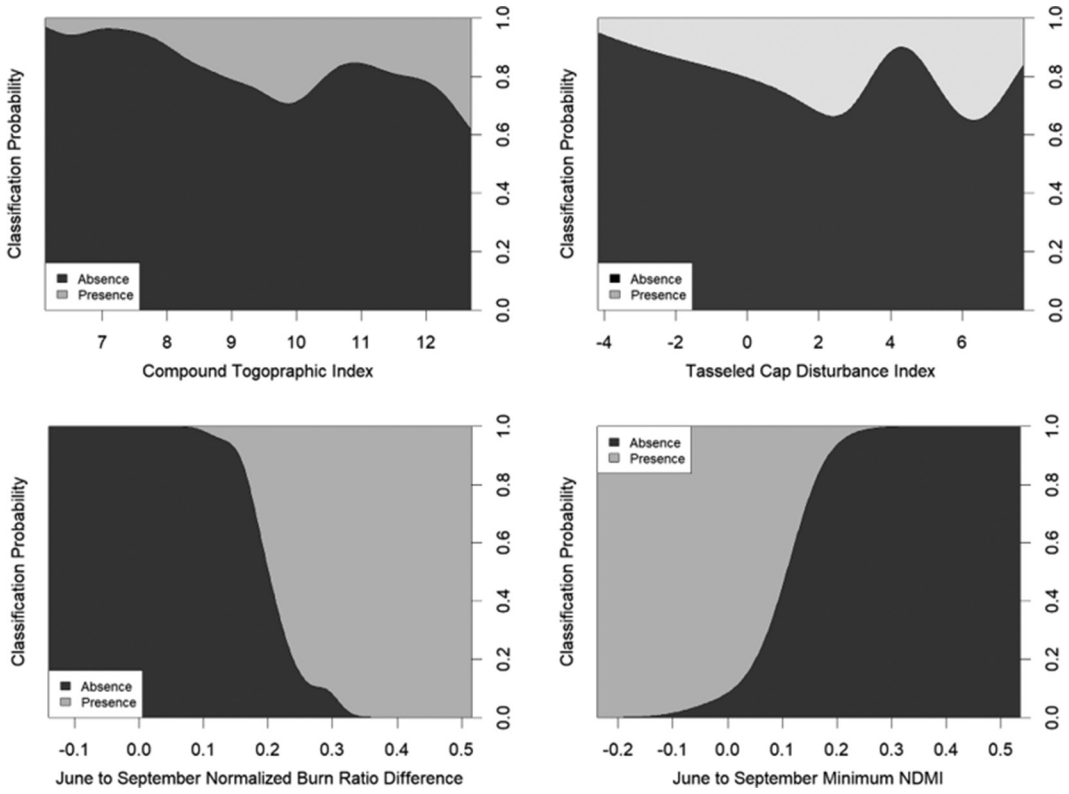

Can. J. For. Res. Downloaded from www.nrcresearchpress.com by UNIVERSITY OF VERMONT on 08/23/19
For personal use only.

Can. J. For. Res. Downloaded from www.nrcresearchpress.com by UNIVERSITY OF VERMONT on 08/23/19
For personal use only.

4. Discussion

The RF model developed in this study effectively classified the presence and absence of black ash dominated stands while addressing potential class imbalance bias. The maps produced are operationally ready estimates of the spatial configuration, distribution, and extent of black ash in northern Minnesota. These results successfully overcome the spatial limitations inherent in using forest inventory data alone to represent local estimates of black ash and allow managers to understand the landscape-level patterns of a species at risk of potential habitat loss due to EAB.

The accuracies presented here are similar to, or improve upon, the limited research generating species-level classifications of black ash from remotely sensed data at the spatial resolution used in this study (30 m). For example, Wolter et al. (1995) used multidate Landsat imagery in a partial least squares (PLS) regression to produce a mean class accuracy of 91% for black ash stands in northwestern Wisconsin after masking all nonhardwood and oak cover types. Wolter and White (2002) used the same methodology and data sources to map black ash cover in northeastern Minnesota (overall accuracy = 83.5%). Again, with a PLS-regression approach and multidate Landsat, Wolter and Townsend (2011) estimated forest composition in northeastern Minnesota and produced a mean accuracy of 89.5% for black ash. Additional studies, focused more on black ash as a component of forest cover type, have generally shown lower classification accuracies. Reese et al. (2002) achieved 81.8% accuracy when combining black ash with red maple (*Acer rubrum* L.) and silver maple (*Acer saccharinum* L.) in a "broad leaf deciduous forest" class while mapping land cover in Wisconsin. A study by Bergen and Dronova (2007) in northern Michigan produced moderate success (accuracy = 75.8%) using a "wet deciduous" category that included trembling aspen (*Populus tremuloides* Michx.), red maple, black ash, and white birch (*Betula papyrifera* Marsh.).

Although direct comparisons cannot be made with the accuracies from models using regression instead of classification, previous studies on abundance have also included black ash at the species level but often at spatial resolutions coarser than those in this study. For example, Chambers et al. (2013) reported an R^2 of 0.37 when estimating black ash basal area across eastern North America using forest inventory data combined with topographic, climate, and soil predictors using 20 km grid cells. Wilson et al. (2013) predicted black ash abundance (R^2 = 0.71) using data from the Moderate Resolution Imaging Spectroradiometer (MODIS; 250 m spatial resolution) across the eastern United States. Studies with similar methodologies using different species have produced higher accuracies compared with this study. Dunckel et al. (2015) reported an AUC value of 0.91 when combining relative basal area from FIA with climatic, soil, and Landsat data in an RF model to classify the presence and absence of a rare forest species (eastern hemlock) in Maine. Evans and Cushman (2009) saw high model performance (AUC ≥ 0.98) for the classification of four conifer species in northern Idaho based on FIA data and a downsampling technique in RF with predictors from topography, climate, and multispectral data.

Overall, the RF classification algorithm produced accurate classifications and generated an interpretable importance metric for each of the predictors used in the final model. The conditional density plot for the most important predictor, CTI, indicated increasing values to be generally associated with an increasing likelihood of presence (Fig. 5). As CTI values increase, drainage depressions tend to form on the landscape, giving the index strong correlations with soil moisture content and surface water pooling (Moore et al. 1991). The ability of CTI to discriminate these topographic features is important in capturing the location of saturated soils (i.e., bogs and streambanks), where few tree species other than black ash can establish or grow (Wright and Rauscher 1990). Furthermore, CTI values for cases in which the probability of presence is higher may be explained by variations in other correlates, including organic matter content, pH, and phosphorus levels (Moore et al. 1993), conducive to black ash establishment. The discriminatory power of CTI is encouraging, but it is also notable that the other derived topographic and soil-moisture indices were less important than hypothesized. This may partially be because of a general lack of landform variation in northern Minnesota relative to areas with complex terrain, where multiple topographic indices have been used to develop species-occurrence models (Evans and Cushman 2009). Additionally, soil-moisture indices may lack precision at higher resolutions, leading to lower model importance (McEachran et al. 2018).

TCAP_DI, a normalized, linear combination of the three standard TC indices (brightness, greenness, and wetness), was also important in the model and displayed a similar trend of values increasing in parallel with the likelihood of presence. Originally developed to highlight the spectral differences between vegetated and unvegetated pixels, TCAP_DI scales from low values representing "mature" forest to high values representing "bare soil" (Healey et al. 2005). In its conditional density plot, higher TCAP_DI values are generally associated with a higher probability of presence (Fig. 5). The most likely explanation is the unique phenology of black ash relative to neighboring deciduous species. Black ash is often the last leaf-on and first leaf-off species (Wolter and Townsend 2011), leading to less light being absorbed by its canopy. Supporting this explanation were the distinct thresholds of the conditional density plots for dNBR and JSmin_NDMI (Fig. 5). For dNBR, high values represent more rapid senescence from April to October and were highly associated with black ash presence. For JSmin_NDMI, presence was associated with low values, which are often found in areas with sparse canopy closure, including forested wetland habitat. The base indices for these two metrics, NBR and NDMI, are both highly influenced by the inclusion of the mid-infrared (MIR) bands, which have shown the ability to discriminate a gradient of foliar moisture content (Hunt et al. 1987).

Though model stability is high in much of the study area, the class probability map indicates that low stability values occur over areas of disturbance, commonly because of forest harvest (Fig. 4). These areas likely account for the notable rate of false positives produced by the model and may be due to unanticipated similarities in photosynthetic activity between areas of forest regrowth and black ash stands or model confusion driven by mixed forest classes generated by aggregating predictors across the extent of the FIA plot (i.e., averaging among subplots). Alternatively, classification confusion could be due to the temporal mismatch between the field data collection period (2011–2015) and the multispectral data (2015 only). To overcome these errors, the use of disturbance metrics from time-series data such as those from LandTrendr (Kennedy et al. 2010) could be used to highlight changes in spectral trajectories indicative of significant vegetation change.

The classification produced in this study can be used to enhance forest management actions at local levels, acting as a complement to additional data sources used to assess the risks to black ash dominated ecosystems posed by EAB. Additionally, the map products may help identify locations for enhanced monitoring efforts investigating the possible factors mitigating EAB impact, including woodpecker habitat use (Flower et al. 2014; Lyons 2015) and the release of biocontrols such as known EAB parasitoids (Duan et al. 2018). The methods presented here could also be applied to models of presence and absence of other ash species across the anticipated invasion range of EAB. Dominant stands identified in this study may also be useful in establishing a baseline of black ash population health (Palik et al. 2012), helping to distinguish between periodic crown dieback and EAB infestation. Finally, these results could also complement the growing body of research assessing the early detection of EAB infestation through remote sensing. Previous work has investigated hyperspectral (Pontius et al. 2008; Zhang et al.

Can. J. For. Res. Downloaded from www.nrcresearchpress.com by UNIVERSITY OF VERMONT on 08/23/19
For personal use only.

2014), LiDAR (Hu et al. 2014), and high spatial resolution data (Murfitt et al. 2016), but approaches utilizing time-series metrics and phenological signatures remain unexplored.

5. Conclusion

Known limitations of systematically collected forest inventory data can be overcome using remotely sensed data in support of forest-species classification and small-area estimation. In this study, we hypothesized that spatially referenced estimates of black ash dominated (>50% basal area) stands in northern Minnesota could be generated by combining FIA survey data with spatial predictors related to soil characteristics and phenology. The class-balanced RF modelling framework presented herein achieved an overall accuracy of 85% and AUC of 0.92 (with class accuracies of 85.4% for absence and 85.7% for presence), indicating robust model performance relative to previous studies conducted with data at similar spatial resolutions. The results support the hypothesis that remote sensing of a finer scale and geospatial products characterizing soils and phenology can extend forest survey data in support of land management actions in smaller management units. The map outputs produced in this study improve upon similar map products at coarse spatial resolutions and can aid local forest managers as they assess EAB risk and vulnerability in black ash dominated stands. Specifically, these map outputs can be paired with hydrology, understory community, and wildlife data to anticipate local ecosystem impacts from the effects of rapid stand mortality due to EAB.

Acknowledgements

This work was supported through funding from the Minnesota Environmental and Natural Resources Trust Fund, Upper Great Lakes and Midwest Landscape Conservation Cooperative, Department of Interior's Northeast Climate Adaptation Science Center, and Colorado State University. Actual plot locations were obtained through a memorandum of understanding (MOU) with the Forest Inventory and Analysis (FIA) Program (USDA Forest Service, Northern Research Station). The authors would like to thank Wilfred Previant of the Colorado State Forest Service for his FIA knowledge and expertise.

References

Alonzo, M., Morton, D.C., Cook, B.D., Andersen, H.E., Babcock, C., and Pattison, R. 2017. Patterns of canopy and surface layer consumption in a boreal forest fire from repeat airborne lidar. Environ. Res. Lett. **12**(6): 065004. doi:10.1088/1748-9326/aa6ade.

Andersen, H.E., Barrett, T., Winterberger, K., Strunk, J., and Temesgen, H. 2009. Estimating forest biomass on the western lowlands of the Kenai Peninsula of Alaska using airborne lidar and field plot data in a model-assisted sampling design. *In* Proceedings of the IUFRO Division 4 Conference: Extending Forest Inventory and Monitoring over Space and Time, Quebec City, Que. pp. 19–22.

Bechtold, W.A., and Patterson, P.L. 2005. The enhanced Forest Inventory and Analysis program — national sampling design and estimation procedures. USDA For. Serv. Gen. Tech. Rep. SRS-80. USDA Forest Service, Southern Research Station, Asheville, N.C. doi:10.2737/SRS-GTR-80.

BenDor, T.K., Metcalf, S.S., Fontenot, L.E., Sangunett, B., and Hannon, B. 2006. Modeling the spread of the Emerald Ash Borer. Ecol. Model. **197**(1–2): 221–236. doi:10.1016/j.ecolmodel.2006.03.003.

Bergen, K.M., and Dronova, I. 2007. Observing succession on aspen-dominated landscapes using a remote sensing-ecosystem approach. Landsc. Ecol. **22**(9): 1395–1410. doi:10.1007/s10980-007-9119-1.

Blackard, J.A., Finco, M.V., Helmer, E.H., Holden, G.R., Hoppus, M.L., Jacobs, D.M., and Ruefenacht, B. 2008. Mapping US forest biomass using nationwide forest inventory data and moderate resolution information. Remote Sens. Environ. **112**(4): 1658–1677. doi:10.1016/j.rse.2007.08.021.

Breiman, L. 2001. Random forests. Mach. Learn. **45**(1): 5–32. doi:10.1023/A:1010933404324.

Chambers, D., Périé, C., Casajus, N., and de Blois, S. 2013. Challenges in modelling the abundance of 105 tree species in eastern North America using climate, edaphic, and topographic variables. For. Ecol. Manage. **291**(1): 20–29. doi:10.1016/j.foreco.2012.10.046.

Chen, C., Liaw, A., and Breiman, L. 2004. Using random forest to learn imbalanced data [online]. University of California, Berkeley. Available from https://statistics.berkeley.edu/sites/default/files/tech-reports/666.pdf [accessed 5 November 2018].

Costanza, K.K.L., Livingston, W.H., Kashian, D.M., Slesak, R.A., Tardif, J.C., Dech, J.P., Diamond, A.K., Daigle, J.J., Ranco, D.J., Neptune, J.S., Benedict, L., Fraver, S.R., Reinikainen, M., and Siegert, N.W. 2017. The precarious state of a cultural keystone species: tribal and biological assessments of the role and future of black ash. J. For. **115**(5): 435–446. doi:10.5849/jof.2016-034R1.

Coulston, J.W., Moisen, G.G., Wilson, B.T., Finco, M.V., Cohen, W.B., and Brewer, C.K. 2012. Modeling percent tree canopy cover: a pilot study. Photogramm. Eng. Remote Sens. **78**(7): 715–727. doi:10.14358/PERS.78.7.715.

Crook, D.J., Khrimian, A., Francese, J.A., Fraser, I., Poland, T.M., Sawyer, A.J., and Mastro, V.C. 2008. Development of a host-based semiochemical lure for trapping emerald ash borer *Agrilus planipennis* (Coleoptera: Buprestidae). Environ. Entomol. **37**(2): 356–365. doi:10.1603/0046-225X(2008)37[356:DOAHSL]2.0.CO;2.

Cutler, D.R., Edwards, T.C., Beard, K.H., Cutler, A., Hess, K.T., Gibson, J., and Lawler, J.J. 2007. Random forests for classification in ecology. Ecology, **88**(11): 2783–2792. doi:10.1890/07-0539.1.

Dahl, T.E., Dick, J., Swords, J., and Wilen, B.O. 2009. Data collection requirements and procedures for mapping wetland, deepwater and related habitats of the United States. National Standards and Support Team, Division of Habitat and Resource Conservation, U.S. Fish and Wildlife Service, Madison, Wis.

D'Amato, A., Palik, B., Slesak, R., Edge, G., Matula, C., and Bronson, D. 2018. Evaluating adaptive management options for black ash forests in the face of emerald ash borer invasion. Forests, **9**(6): 348. doi:10.3390/f9060348.

DeSantis, R.D., Moser, W.K., Gormanson, D.D., Bartlett, M.G., and Vermunt, B. 2013. Effects of climate on emerald ash borer mortality and the potential for ash survival in North America. Agric. For. Meteorol. **178**: 120–128. doi:10.1016/j.agrformet.2013.04.015.

Diamond, J.S., McLaughlin, D., Slesak, R., D'Amato, A., and Palik, B. 2018. Forested versus herbaceous wetlands: can management mitigate ecohydrologic regime shifts from invasive emerald ash borer? J. Environ. Manage. **222**: 436–446. doi:10.1016/j.jenvman.2018.05.082.

Drummond, C., and Holte, R.C. 2003. C4.5, class imbalance, and cost sensitivity: why under-sampling beats over-sampling [online]. *In* Workshop on Learning from Imbalanced Datasets II. Available from http://www.site.uottawa.ca/~nat/Workshop2003/drummondc.pdf [accessed 5 November 2018].

Duan, J., Bauer, L., van Driesche, R., and Gould, J. 2018. Progress and challenges of protecting North American ash trees from the emerald ash borer using biological control. Forests, **9**(3): 142. doi:10.3390/f9030142.

Dunckel, K., Weiskittel, A., Fiske, G., Sader, S.A., Latty, E., and Arnett, A. 2015. Linking remote sensing and various site factors for predicting the spatial distribution of eastern hemlock occurrence and relative basal area in Maine, USA. For. Ecol. Manage. **358**: 180–191. doi:10.1016/j.foreco.2015.09.012.

Duveneck, M.J., Thompson, J.R., and Wilson, B.T. 2015. An imputed forest composition map for New England screened by species range boundaries. For. Ecol. Manage. **347**: 107–115. doi:10.1016/j.foreco.2015.03.016.

Ellison, A.M., Bank, M.S., Clinton, B.D., Colburn, E.A., Elliott, K., Ford, C.R., Foster, D.R., Kloeppel, B.D., Knoepp, J.D., Lovett, G.M., Mohan, J., Orwig, D.A., Rodenhouse, N.L., Sobczak, W.V., Stinson, K.A., Stone, J.K., Swan, C.M., Thompson, J., Von Holle, B., and Webster, J.R. 2005. Loss of foundation species: consequences for the structure and dynamics of forested ecosystems. Front. Ecol. Environ. **3**(9): 479–486. doi:10.1890/1540-9295(2005)003[0479:LOFSCF]2.0.CO;2.

Evans, J.S., and Cushman, S.A. 2009. Gradient modeling of conifer species using random forests. Landsc. Ecol. **24**(5): 673–683. doi:10.1007/s10980-009-9341-0.

Evans, J.S., Hudak, A.T., Faux, R., and Smith, A. 2009. Discrete return lidar in natural resources: recommendations for project planning, data processing, and deliverables. Remote Sens. **1**(4): 776–794. doi:10.3390/rs1040776.

Evans, J.S., Murphy, M.A., Holden, Z.A., and Cushman, S.A. 2011. Modeling species distribution and change using random forest. *In* Predictive species and habitat modeling in landscape ecology: concepts and applications. *Edited by* C.A. Drew, Y.F. Wiersma, and F. Huettmann. Springer, New York. pp. 153–159. doi:10.1007/978-1-4419-7390-0_8.

Falkowski, M.J., Evans, J.S., Martinuzzi, S., Gessler, P.E., and Hudak, A.T. 2009. Characterizing forest succession with lidar data: an evaluation for the Inland Northwest, USA. Remote Sens. Environ. **113**(5): 946–956. doi:10.1016/j.rse.2009.01.003.

Flower, C.E., Knight, K.S., and Gonzalez-Meler, M.A. 2013. Impacts of the emerald ash borer (*Agrilus planipennis* Fairmaire) induced ash (*Fraxinus* spp.) mortality on forest carbon cycling and successional dynamics in the eastern United States. Biol. Invasions, **15**(4): 931–944. doi:10.1007/s10530-012-0341-7.

Flower, C.E., Long, L.C., Knight, K.S., Rebbeck, J., Brown, J.S., Gonzalez-Meler, M.A., and Whelan, C.J. 2014. Native bark-foraging birds preferentially forage in infected ash (*Fraxinus* spp.) and prove effective predators of the invasive emerald ash borer (*Agrilus planipennis* Fairmaire). For. Ecol. Manage. **313**: 300–306. doi:10.1016/j.foreco.2013.11.030.

Gandhi, K.J.K., and Herms, D.A. 2010. Direct and indirect effects of alien insect herbivores on ecological processes and interactions in forests of eastern North America. Biol. Invasions, **12**(2): 389–405. doi:10.1007/s10530-009-9627-9.

Goerndt, M.E., Monleon, V.J., and Temesgen, H. 2013. Small-area estimation of county-level forest attributes using ground data and remote sensed auxiliary information. For. Sci. **59**(5): 536–548. doi:10.5849/forsci.12-073.

He, H., and Garcia, E.A. 2009. Learning from imbalanced data. IEEE Trans. Knowl. Data Eng. **21**(9): 1263–1284. doi:10.1109/TKDE.2008.239.

Healey, S.P., Cohen, W.B., Zhiqiang, Y., and Krankina, O.N. 2005. Comparison of

Can. J. For. Res. Downloaded from www.nrcresearchpress.com by UNIVERSITY OF VERMONT on 08/23/19
For personal use only.

Tasseled Cap-based Landsat data structures for use in forest disturbance detection. Remote Sens. Environ. **97**(3): 301–310. doi:10.1016/j.rse.2005.05.009.

Herms, D.A., and McCullough, D.G. 2014. Emerald ash borer invasion of North America: history, biology, ecology, impacts, and management. Annu. Rev. Entomol. **59**(1): 13–30. doi:10.1146/annurev-ento-011613-162051.

Hu, B., Li, J., Wang, J., and Hall, B. 2014. The early detection of the emerald ash borer (EAB) using advanced geospacial technologies. Int. Arch. Photogramm. Remote Sens. Spatial Inf. Sci. **40**(2): 213–219. doi:10.5194/isprsarchives-XL-2-213-2014.

Hunt, E.R., Rock, B.N., and Nobel, P.S. 1987. Measurement of leaf relative water content by infrared reflectance. Remote Sens. Environ. **22**(3): 429–435. doi:10.1016/0034-4257(87)90094-0.

Iverson, L.R., Dale, M.E., Scott, C.T., and Prasad, A. 1997. A GIS-derived integrated moisture index to predict forest composition and productivity of Ohio forests (U.S.A.). Landsc. Ecol. **12**(5): 331–348. doi:10.1023/A:1007989813501.

Japkowicz, N., and Stephen, S. 2002. The class imbalance problem: a systematic study. Intell. Data Anal. **6**(5): 429–449. doi:10.3233/IDA-2002-6504.

Kenis, M., Auger-Rozenberg, M.-A., Roques, A., Timms, L., Péré, C., Cock, M.J.W., Settele, J., Augustin, S., and Lopez-Vaamonde, C. 2009. Ecological effects of invasive alien insects. *In* Ecological impacts of non-native invertebrates and fungi on terrestrial ecosystems. *Edited by* D. Langor and J. Sweeney. Springer, Dordrecht, Netherlands. pp. 21–45. doi:10.1007/978-1-4020-9680-8_3.

Kennedy, R.E., Yang, Z., and Cohen, W.B. 2010. Detecting trends in forest disturbance and recovery using yearly Landsat time series: 1. LandTrendr — temporal segmentation algorithms. Remote Sens. Environ. **114**(12): 2897–2910. doi:10.1016/j.rse.2010.07.008.

Klooster, W.S., Herms, D.A., Knight, K.S., Herms, C.P., McCullough, D.G., Smith, A., Gandhi, K.J.K., and Cardina, J. 2014. Ash (*Fraxinus* spp.) mortality, regeneration, and seed bank dynamics in mixed hardwood forests following invasion by emerald ash borer (*Agrilus planipennis*). Biol. Invasions, **16**(4): 859–873. doi:10.1007/s10530-013-0543-7.

Knight, K.S., Brown, J.P., and Long, R.P. 2013. Factors affecting the survival of ash (*Fraxinus* spp.) trees infested by emerald ash borer (*Agrilus planipennis*). Biol. Invasions, **15**(2): 371–383. doi:10.1007/s10530-012-0292-z.

Kovacs, K.F., Mercader, R.J., Haight, R.G., Siegert, N.W., McCullough, D.G., and Liebhold, A.M. 2011. The influence of satellite populations of emerald ash borer on projected economic costs in U.S. communities, 2010–2020. J. Environ. Manage. **92**(9): 2170–2181. doi:10.1016/j.jenvman.2011.03.043.

Liang, L., and Fei, S. 2014. Divergence of the potential invasion range of emerald ash borer and its host distribution in North America under climate change. Clim. Change, **122**(4): 735–746. doi:10.1007/s10584-013-1024-9.

Liaw, A., and Wiener, M. 2002. Classification and regression by randomForest [online]. R News, **2/3**(December 2002): 18–22. Available from https://cran.r-project.org/doc/Rnews/Rnews_2002-3.pdf [accessed 5 November 2018].

Liu, W., Song, C., Schroeder, T.A., and Cohen, W.B. 2008. Predicting forest successional stages using multitemporal Landsat imagery with forest inventory and analysis data. Int. J. Remote Sens. **29**(13): 3855–3872. doi:10.1080/01431160701840166.

Looney, C.E., D'Amato, A.W., Palik, B.J., Slesak, R.A., and Slater, M.A. 2017. The response of *Fraxinus nigra* forest ground-layer vegetation to emulated emerald ash borer mortality and management strategies in northern Minnesota, USA. For. Ecol. Manage. **389**(2017): 352–363. doi:10.1016/j.foreco.2016.12.028.

Lovett, G.M., Weiss, M., Liebhold, A.M., Holmes, T.P., Leung, B., Lambert, K.F., Orwig, D.A., Campbell, F.T., Rosenthal, J., McCullough, D.G., Wildova, R., Ayres, M.P., Canham, C.D., Foster, D.R., LaDeau, S.L., and Weldy, T. 2016. Nonnative forest insects and pathogens in the United States: impacts and policy options. Ecol. Appl. **26**(5): 1437–1455. doi:10.1890/15-1176.

Lyons, D.B. 2015. What's killing the green menace: mortality factors affecting the emerald ash borer (Coleoptera: Buprestidae) in North America? Can. Entomol. **147**(3): 263–276. doi:10.4039/tce.2014.62.

Martin, M.E., Newman, S.D., Aber, J.D., and Congalton, R.G. 1998. Determining forest species composition using high spectral resolution remote sensing data. Remote Sens. Environ. **65**(3): 249–254. doi:10.1016/S0034-4257(98)00035-2.

McCune, B., and Keon, D. 2002. Equations for potential annual direct incident radiation and heat load. J. Veg. Sci. **13**(4): 603–606. doi:10.1111/j.1654-1103.2002.tb02087.x.

McEachran, Z.P., Slesak, R.A., and Karwan, D.L. 2018. From skid trails to landscapes: vegetation is the dominant factor influencing erosion after forest harvest in a low relief glaciated landscape. For. Ecol. Manage. **430**: 299–311. doi:10.1016/j.foreco.2018.08.021.

McRoberts, R.E. 2009. A two-step nearest neighbors algorithm using satellite imagery for predicting forest structure within species composition classes. Remote Sens. Environ. **113**(3): 532–545. doi:10.1016/j.rse.2008.10.001.

McRoberts, R.E., and Tomppo, E.O. 2007. Remote sensing support for national forest inventories. Remote Sens. Environ. **110**(4): 412–419. doi:10.1016/j.rse.2006.09.034.

Minnesota Department of Natural Resources. 2017. Ecological Classification System: Laurentian Mixed Forest Province [online]. Available from http://www.dnr.state.mn.us/ecs/212/index.html [accessed 25 April 2017].

MNGeo. 2017. Metadata: LiDAR elevation, Arrowhead Region, NE Minnesota, 2011 [online]. Minnesota Department of Natural Resources. Available from http://www.mngeo.state.mn.us/chouse/metadata/lidar_arrowhead2011.html [accessed 25 April 2017].

Moisen, G.G., Freeman, E.A., Blackard, J.A., Frescino, T.S., Zimmermann, N.E., and Edwards, T.C. 2006. Predicting tree species presence and basal area in Utah: a comparison of stochastic gradient boosting, generalized additive models, and tree-based methods. Ecol. Model. **199**(2): 176–187. doi:10.1016/j.ecolmodel.2006.05.021.

Moore, I.D., Grayson, R.B., and Ladson, A.R. 1991. Digital terrain modelling: a review of hydrological, geomorphological, and biological applications. Hydrol. Proccess. **5**(1): 3–30. doi:10.1002/hyp.3360050103.

Moore, I.D., Gessler, P.E., Nielsen, G.A., and Peterson, G.A. 1993. Soil attribute prediction using terrain analysis. Soil Sci. Soc. Am. J. **57**(2): 443–452. doi:10.2136/sssaj1993.03615995005700020026x.

Murfitt, J., He, Y., Yang, J., Mui, A., and De Mille, K. 2016. Ash decline assessment in emerald ash borer infested natural forests using high spatial resolution images. Remote Sens. **8**(3): 256. doi:10.3390/rs8030256.

Murphy, M.A., Evans, J.S., and Storfer, A. 2010. Quantifying *Bufo boreas* connectivity in Yellowstone National Park with landscape genetics. Ecology, **91**(1): 252–261. doi:10.1890/08-0879.1.

Nelson, M.D., Healey, S.P., Moser, W.K., and Hansen, M.H. 2009. Combining satellite imagery with forest inventory data to assess damage severity following a major blowdown event in northern Minnesota, USA. Int. J. Remote Sens. **30**(19): 5089–5108. doi:10.1080/01431160903022951.

Ohmann, J.L., and Gregory, M.J. 2002. Predictive mapping of forest composition and structure with direct gradient analysis and nearest-neighbor imputation in coastal Oregon, U.S.A. Can. J. For. Res. **32**(4): 725–741. doi:10.1139/x02-011.

Olaya-Marín, E.J., Martínez-Capel, F., and Vezza, P. 2013. A comparison of artificial neural networks and random forests to predict native fish species richness in Mediterranean rivers. Knowl. Manage. Aquat. Ecosyst. **409**(7): 19. doi:10.1051/kmae/2013052.

Palik, B.J., Ostry, M.E., Venette, R.C., and Abdela, E. 2012. Tree regeneration in black ash (*Fraxinus nigra*) stands exhibiting crown dieback in Minnesota. For. Ecol. Manage. **269**: 26–30. doi:10.1016/j.foreco.2011.12.020.

Poland, T.M., and McCullough, D.G. 2006. Emerald ash borer: invasion of the urban forest and the threat to North America's ash resource. J. For. **104**(3): 118–124.

Pontius, J., Martin, M., Plourde, L., and Hallett, R. 2008. Ash decline assessment in emerald ash borer-infested regions: a test of tree-level, hyperspectral technologies. Remote Sens. Environ. **112**(5): 2665–2676. doi:10.1016/j.rse.2007.12.011.

Powell, S.L., Cohen, W.B., Healey, S.P., Kennedy, R.E., Moisen, G.G., Pierce, K.B., and Ohmann, J.L. 2010. Quantification of live aboveground forest biomass dynamics with Landsat time-series and field inventory data: a comparison of empirical modeling approaches. Remote Sens. Environ. **114**(5): 1053–1068. doi:10.1016/j.rse.2009.12.018.

R Core Team. 2017. R: a language and environment for statistical computing [online]. R Foundation for Statistical Computing, Vienna, Austria. Available from https://www.R-project.org/.

Reese, H.M., Lillesand, T.M., Nagel, D.E., Stewart, J.S., Goldmann, R.A., Simmons, T.E., Chipman, J.W., and Tessar, P.A. 2002. Statewide land cover derived from multiseasonal Landsat TM data: a retrospective of the WISCLAND project. Remote Sens. Environ. **82**(2–3): 224–237. doi:10.1016/S0034-4257(02)00039-1.

Schroeder, T.A., Healey, S.P., Moisen, G.G., Frescino, T.S., Cohen, W.B., Huang, C., Kennedy, R.E., and Yang, Z. 2014. Improving estimates of forest disturbance by combining observations from Landsat time series with U.S. Forest Service Forest Inventory and Analysis data. Remote Sensing of Environment, **154**(November): 61–73. doi:10.1016/j.rse.2014.08.005.

Sheridan, R., Popescu, S., Gatziolis, D., Morgan, C., and Ku, N.-W. 2014. Modeling forest aboveground biomass and volume using airborne LiDAR metrics and forest inventory and analysis data in the Pacific Northwest. Remote Sens. **7**(1): 229–255. doi:10.3390/rs70100229.

Slesak, R.A., Lenhart, C.F., Brooks, K.N., D'Amato, A.W., and Palik, B.J. 2014. Water table response to harvesting and simulated emerald ash borer mortality in black ash wetlands in Minnesota, USA. Can. J. For. Res. **44**(8): 961–968. doi:10.1139/cjfr-2014-0111.

Soil Survey Staff. 2017. Gridded Soil Survey Geographic (gSSURGO) Database for Minnesota [online]. United States Department of Agriculture, Natural Resources Conservation Service. Available from https://gdg.sc.egov.usda.gov [accessed 5 November 2018].

Taylor, R.A.J., Bauer, L.S., Poland, T.M., and Windell, K.N. 2010. Flight performance of *Agrilus planipennis* (Coleoptera: Buprestidae) on a flight mill and in free flight. J. Insect Behav. **23**(2): 128–148. doi:10.1007/s10905-010-9202-3.

Telander, A.C., Slesak, R.A., D'Amato, A.W., Palik, B.J., Brooks, K.N., and Lenhart, C.F. 2015. Sap flow of black ash in wetland forests of northern Minnesota, USA: hydrologic implications of tree mortality due to emerald ash borer. Agric. For. Meteorol. **206**: 4–11. doi:10.1016/j.agrformet.2015.02.019.

Tinkham, W.T., Smith, A., Marshall, H., Link, T.E., Falkowski, M.J., and Winstral, A.M. 2014. Quantifying spatial distribution of snow depth errors from LiDAR using random forest. Remote Sens. Environ. **141**: 105–115. doi:10.1016/j.rse.2013.10.021.

U.S. Geological Survey. 2017. Earth Resources Observation and Science (EROS) Center Science Processing Architecture (ESPA) on Demand Interface [online]. Product Guide Version 4.0. Department of Interior, U.S. Geological Survey.

Available from https://landsat.usgs.gov/sites/default/files/documents/espa_odi_userguide.pdf [accessed 5 April 2017].
Vogeler, J.C., Braaten, J.D., Slesak, R.A., and Falkowski, M.J. 2018. Extracting the full value of the Landsat archive: inter-sensor harmonization for the mapping of Minnesota forest canopy cover (1973–2015). Remote Sens. Environ. **209**: 363–374. doi:10.1016/j.rse.2018.02.046.
Willow, A.J. 2011. Indigenizing invasive species management: Native North Americans and the emerald ash borer (EAB) beetle. Cult. Agric. Food Environ. **33**(2): 70–82. doi:10.1111/j.2153-9561.2011.01051.x.
Wilson, B.T., Lister, A.J., Riemann, R.I., and Griffith, D.M. 2013. Live tree species basal area of the contiguous United States (2000–2009). USDA Forest Service, Rocky Mountain Research Station, Newtown Square, PA. doi:10.2737/RDS-2013-0013.
Wolter, P.T., and Townsend, P.A. 2011. Multi-sensor data fusion for estimating forest species composition and abundance in northern Minnesota. Remote Sens. Environ. **115**(2): 671–691. doi:10.1016/j.rse.2010.10.010.
Wolter, P.T., and White, M.A. 2002. Recent forest cover type transitions and landscape structural changes in northeast Minnesota, USA. Landsc. Ecol. **17**(2): 133–155. doi:10.1023/A:1016522509857.
Wolter, P.T., Mladenoff, D.J., Host, G.E., and Crow, T.R. 1995. Improved forest classification in the northern Lake States using multi-temporal Landsat imagery. Photogram. Eng. Remote Sens. **61**(9): 1129–1143.
Wright, J.W., and Rauscher, H.M. 1990. *Fraxinus nigra* Marsh. black ash [online]. *In* Silvics of North America: Volume 2. Hardwoods. *Edited by* R.M. Burns and B.H. Honkala. USDA Forest Service, Washington, D.C. pp. 344–347. Available from https://www.na.fs.fed.us/spfo/pubs/silvics_manual/volume_2/fraxinus/nigra.htm [accessed 5 November 2018].
Youngquist, M.B., Eggert, S.L., D'Amato, A.W., Palik, B.J., and Slesak, R.A. 2017. Potential effects of foundation species loss on wetland communities: a case study of black ash wetlands threatened by emerald ash borer. Wetlands, **37**(4): 787–799. doi:10.1007/s13157-017-0908-2.
Zhang, K., Hu, B., and Robinson, J. 2014. Early detection of emerald ash borer infestation using multisourced data: a case study in the town of Oakville, Ontario, Canada. J. Appl. Remote Sens. **8**(1): 83602. doi:10.1117/1.JRS.8.083602.
Zimmermann, N.E., Edwards, T.C., Moisen, G.G., Frescino, T.S., and Blackard, J.A. 2007. Remote sensing-based predictors improve distribution models of rare, early successional, and broadleaf tree species in Utah. J. Appl Ecol. **44**(5): 1057–1067. doi:10.1111/j.1365-2664.2007.01348.x.

Can. J. For. Res. Downloaded from www.nrcresearchpress.com by UNIVERSITY OF VERMONT on 08/23/19
For personal use only.